Evaluating Four Multisatellite Precipitation Estimates over the Diaoyu Islands during Typhoon Seasons

BIN YONG,*,+ JINGJING WANG,+ LILIANG REN,* YALEI YOU,# PINGPING XIE,@ AND YANG HONG&

* *State Key Laboratory of Hydrology-Water Resources and Hydraulic Engineering, Hohai University, Nanjing, China*
+ *School of Earth Sciences and Engineering, Hohai University, Nanjing, China,*
# *Cooperative Institute for Climate and Satellites, Earth System Science Interdisciplinary Center, University of Maryland, College Park, College Park, Maryland*
@ *NOAA/NWS/NCEP/Climate Prediction Center, College Park, Maryland*
& *School of Civil Engineering and Environmental Sciences, University of Oklahoma, Norman, Oklahoma*

(Manuscript received 11 September 2015, in final form 3 February 2016)

ABSTRACT

The Diaoyu Islands are a group of uninhabited islets located in the East China Sea between Japan, China, and Taiwan. Here, four mainstream gauge-adjusted multisatellite precipitation estimates [TRMM Multisatellite Precipitation Analysis, version 7 (TMPA-V7); CPC morphing technique–bias-corrected product (CMORPH-CRT); Precipitation Estimation from Remotely Sensed Information Using Artificial Neural Networks–Climate Data Record (PERSIANN-CDR); and Global Satellite Mapping of Precipitation–gauge adjusted (GSMaP_Gauge)] are adopted to detect the rainfall characteristics of the Diaoyu Islands area with a particular focus on typhoon contribution. Out of the four products, CMORPH-CRT and GSMaP_Gauge show much more similarity both in terms of the spatial patterns and error structures because of their use of the same morphing technique. Overall, GSMaP_Gauge performs better than the other three products, likely because of denser in situ observations integrated in its retrieval algorithms over East Asia. All rainfall products indicate that an apparent rain belt exists along the northeastern 45° direction of Taiwan extending to Kyushu of Japan, which is physically associated with the Kuroshio. The Diaoyu Islands are located on the central axis of this rain belt. During the period 2001–09, typhoon-induced rainfall accounted for 530 mm yr^{-1}, and typhoons contributed on average approximately 30% of the annual precipitation budget over the Diaoyu Islands. Higher typhoon contribution was found over the southern warmer water of the Diaoyu Islands, while the northern cooler water presented less contribution ratio. Supertyphoon Chaba, the largest typhoon of 2004, recorded 53 h of rainfall accumulation totaling 235 mm on the Diaoyu Islands, and this event caused severe property damage and human casualties for Japan. Hence, the Diaoyu Islands play an important role in weather monitoring and forecasting for the neighboring countries and regions.

1. Introduction

The Diaoyu Islands, also called the Diaoyutai Islands in Taiwan or the Senkaku Islands in Japan, are a clutch of five small volcanic islets and three rocky outcroppings in the East China Sea. The largest of them, Diaoyu Island, has an area of just 4.38 km^2 and is 383 m above sea level at its highest point (Fig. 1). This islet lies at 25°44′30″N latitude and 123°28′30″E longitude, approximately 170 km northeast of Taiwan, 330 km east of mainland China, and 410 km west of Okinawa Island, Japan. It is the only islet suitable for weather station mounting in this uninhabited island chain. In practice, the western Pacific tropical cyclones frequently passed through this region and brought a large amount of rainfall along the typhoon tracks, resulting in severe property damage and human casualties, especially for Taiwan, Japan, and the eastern coastline of mainland China. Diaoyu Island plays an important meteorological outpost role for the surrounding countries and has great potential in regional weather monitoring and forecasting, besides the military and economic values. Up to now, however, there has not been any meteorological equipment installed on Diaoyu Island.

As is well known, precipitation is one of the crucial atmospheric variables for weather monitoring and forecasting. Despite its importance, accurate rainfall measurement remains challenging, especially over oceans

Corresponding author address: Bin Yong, State Key Laboratory of Hydrology-Water Resources and Hydraulic Engineering, Hohai University, Xikang Road 1, Nanjing 210098, China.
E-mail: yongbin_hhu@126.com; rll@hhu.edu.cn

DOI: 10.1175/JHM-D-15-0165.1

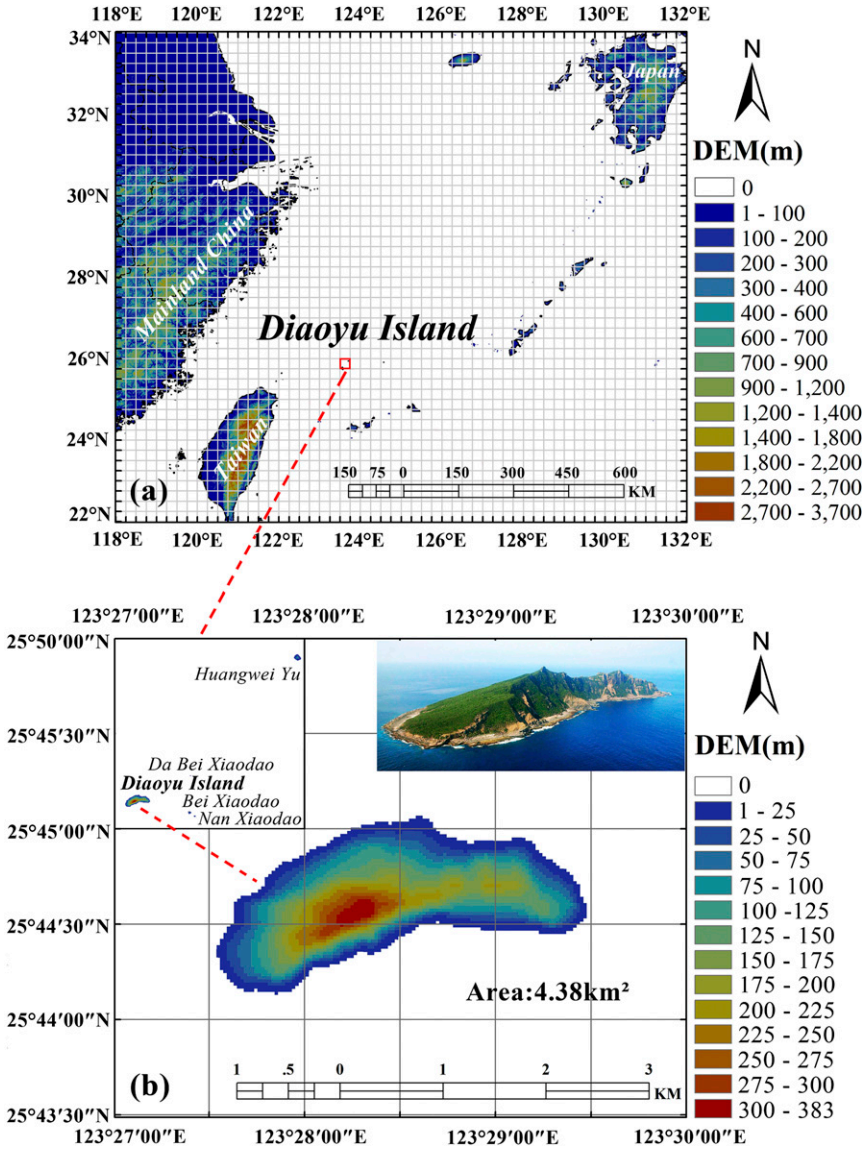

FIG. 1. (a) Location of the study domain and (b) topography of the Diaoyu Islands.

and islands because of the sparse in situ observations from islets or buoys. Over the past few years, we have witnessed rapid developments in the field of satellite-based precipitation estimation, which might be the only practical way to detect and offer precipitation information for ungauged remote regions such as the Diaoyu Islands and their adjacent sea (Sorooshian et al. 2000; Joyce et al. 2004; Kubota et al. 2007; Tapiador et al. 2012; Yong et al. 2015). At present, highlighted advancements in satellite precipitation estimates have crystallized into the Global Precipitation Measurement (GPM) mission that can unify and improve the precipitation measurements by a constellation of research and operational microwave sensors to set a new calibration standard for the global precipitation estimation from space (Hou et al. 2014). The GPM Core Observatory, with a dual-frequency precipitation radar (DPR) and a multichannel GPM Microwave Imager (GMI), was successfully launched by NASA and JAXA on 28 February 2014. However, the U.S.–Japan data producers are unable to provide GPM-calibrated historic precipitation records for the pre-2014 period, when DPR and GMI observations were not yet available. As the predecessor to GPM, the Tropical Rainfall Measuring Mission (TRMM), launched in November 1997, has generated over 17 years of valuable scientific data. The TRMM-based multisatellite estimates

are the current mainstream satellite precipitation measurements at the global scale, and they improved our comprehensive understanding of Earth's water and energy cycle, tropical cyclone structure and evolution, convective system properties, lightning–storm relationships, and human impacts on rainfall. Examples of these operational quasi-global rainfall products are the TRMM Multisatellite Precipitation Analysis (TMPA; Huffman et al. 2007, 2009), the NOAA/Climate Prediction Center (CPC) morphing technique (CMORPH; Joyce et al. 2004), Precipitation Estimation from Remotely Sensed Information Using Artificial Neural Networks (PERSIANN; Hsu et al. 1997; Sorooshian et al. 2000), and the JAXA's Global Satellite Mapping of Precipitation (GSMaP; Kubota et al. 2007). The concept behind most of these algorithms relies upon the merged passive microwave (PMW) and infrared (IR) estimates. Generally, the more accurate (but infrequent) PMW estimates were used to calibrate the more frequent (but indirect physical relations with precipitation) IR estimates so that the retrieval system could provide not only better estimates, but estimates at improved temporal and spatial resolutions. After merging PMW- and IR-based estimates, the rain gauge measurement information would be integrated into the retrieval systems to produce the research-quality, post-real-time products. To date, these merged high-resolution satellite precipitation products have been widely utilized in various research and operational applications with positive performance (e.g., Villarini and Krajewski 2007; Su et al. 2008; Habib et al. 2009; Tobin and Bennett 2010; Yong et al. 2010; Romilly and Gebremichael 2011; Bitew et al. 2012; Khan et al. 2012; Wu et al. 2012). By providing global and consistent spatial coverage, satellite precipitation estimates allow the opportunity to monitor the structure of tropical cyclones and to quantify the associated rainfall amount over the ungauged areas. However, most recent literature mainly focused on the global and continental scales (Rodgers et al. 2001; McCollum et al. 2002; Lonfat et al. 2004; Yu et al. 2009; Nogueira and Kleim 2011; Dare et al. 2012; Prat and Nelson 2013; Villarini et al. 2014; Bowman and Fowler 2015). The regional studies with small- and medium-sized scales that include different satellite precipitation estimates over the ungauged regions are seldom found.

The aim of this study is to investigate the rainfall characteristics of the Diaoyu Islands and their adjacent sea from space, with a particular focus on the contribution of typhoon rainfall. For that purpose, four mainstream multisatellite precipitation products are used. The evaluation is performed for a complete 9-yr period (2001–09). This study is expected to offer a better understanding of local weather and hydrology features over this ungauged island chain for its neighboring countries and regions.

2. Data

a. Satellite datasets

Previous studies have shown that the gauge-adjusted satellite precipitation products are more accurate than their unadjusted counterparts, as the widely used month-to-month gauge adjustments successfully remove systematic biases of purely satellite-derived estimates (Stisen and Sandholt 2010; Yong et al. 2010; Bitew and Gebremichael 2011; Chen et al. 2013a,b). Furthermore, it was also found that such a bias-adjustment scheme can yield substantial improvements in capturing both spatial patterns and temporal variations of precipitation (Shen et al. 2010; Behrangi et al. 2011). Therefore, four gauge-adjusted satellite estimates [TMPA, version 7 (TMPA-V7); CMORPH–bias-corrected product (CMORPH-CRT); PERSIANN–Climate Data Record (PERSIANN-CDR); and GSMaP–gauge adjusted (GSMaP_Gauge)] are considered for the analyses.

During the past decade, the TMPA system has undergone three major upgrades (corresponding to versions 5, 6, and 7) owing to the new sensors and upgraded algorithms (Yong et al. 2013). The standard TMPA estimates are provided at relatively fine resolution (0.25° × 0.25°, 3-hourly) in both real (3B42RT) and post–real time (3B42). TMPA-V7 is the latest version 7 research-grade 3B42 product of TMPA released on 28 January 2013 (Huffman and Bolvin 2015). Against the original version 6, the new version 7 has substantial upgrades: 1) employing the significantly improved Global Precipitation Climatology Centre (GPCC), version 2.2, dataset as its full gauge analysis and bias adjustments; 2) introducing some newer microwave and infrared sensors, mainly the Special Sensor Microwave Imager/Sounder (SSMIS) on the *F16* and *F17* satellites, the Microwave Humidity Sounder (MHS) on *NOAA-18* and *NOAA-19*, Meteorological Operation (MetOp), and the 0.07° Gridded Satellite (GridSat-B1) IR brightness temperature (TB) data; 3) uniformly processing the input data, most notably for AMSU and MHS, but also including TRMM Combined Instrument (TCI), TMI, AMSR-E, and SSM/I; 4) adopting a latitude-band calibration scheme for all satellites; and 5) adding new fields in the data files (sensor-specific source and overpass time). Generally, TMPA-V7 is considered an improvement over TMPA-V6, and it apparently outperforms all of its previous versions (e.g., Yong et al. 2014; Chen et al. 2013a,b). The TMPA-V7 dataset can be downloaded from the website of the Goddard Earth Sciences Data and Information Services Center (http://disc.sci.gsfc.nasa.gov/gesNews/trmm_v7_multisat_precip).

The CMORPH estimates adopt motion vectors derived from half-hourly interval geostationary satellite IR imagery to propagate the relatively high-quality precipitation

estimates derived from passive microwave data (Joyce et al. 2004). In the CMORPH algorithm, the shape and intensity of the precipitation features are morphed during the time between microwave sensor scans by performing a time-weighted linear interpolation. Altogether, CMORPH consists of two successive versions, namely, the original version 0.x and the current version 1.0. Relative to the old version, the latest CMORPH (version 1.0) uses a fixed algorithm and inputs of fixed versions to ensure the best possible homogeneity throughout the entire TRMM era. Moreover, version 1.0 includes a bias-corrected product (CMORPH-CRT) as well as the raw, purely satellite-derived precipitation estimates (CMORPH-RAW), while version 0.x only has the latter (Xie and Xiong 2011). As for CMORPH-CRT and CMORPH-RAW, three different spatiotemporal resolutions (i.e., 8 km, 30 min; 0.25°, 3-hourly; and 0.25°, daily) were made available starting on 1 January 1998 (from http://ftp.cpc.ncep.noaa.gov/precip/CMORPH_V1.0/). The 0.25° 3-hourly bias-adjusted CMORPH-CRT data were used in this study.

PERSIANN-CDR is a new retrospective satellite-based precipitation dataset developed from the PERSIANN algorithm that estimates rainfall distribution from infrared geostationary satellite imagery by using the artificial neural network (Ashouri et al. 2015). First, the GridSat-B1 infrared data are applied in the PERSIANN model to produce historical rainfall estimates. These estimates are then bias adjusted with the Global Precipitation Climatology Project (GPCP) 2.5° monthly data, which include the GPCC gauge information. PERSIANN-CDR provides a 32-yr record (from 1 January 1983 to 31 December 2014) of near-global (60°S–60°N) daily precipitation data at 0.25° spatial resolution (available at ftp://data.ncdc.noaa.gov/cdr/persiann/files/). This new product is aimed at addressing the need for a consistent, high-resolution, and global climate data record for studying long-term hydrometeorology features in daily precipitation, especially extreme precipitation events at regional and global scales.

The GSMaP algorithm combines precipitation retrievals from TRMM and other polar satellites and interpolates them with cloud-moving vectors derived from IR images of geostationary satellites to produce high-resolution (0.1°, 1-hourly) global precipitation estimates for the latitude band 60°N–60°S (Kubota et al. 2007; Okamoto et al. 2008; Aonashi et al. 2009). In addition to the routine satellite input streams, two additional data sources were employed in GSMaP's PWM algorithms: 1) Japan Meteorological Agency (JMA) Global Analysis (GANAL) data (1.25°, 6-hourly) and 2) JMA Merged Satellite and in situ Data Global Daily Sea Surface Temperatures (MGDSST; 1°, daily). First, Kubota et al. (2007) developed a simplified, near-real-time version of GSMaP (GSMaP_NRT), which uses fewer PMW input streams and a forward-only cloud advection scheme. In practice, GSMaP_NRT seems to be more similar to CMORPH, as it inherits CMORPH's morphing algorithm to derive cloud motion vectors. To further reduce the total retrieval errors, Ushio et al. (2009) employed a new Kalman filter approach to assimilate and refine the IR-based rain rates and thus generated an improved version [GSMaP moving vector with Kalman filter (GSMaP_MVK)] with almost all available satelliteborne precipitation-related sensors. Another important difference between these two GSMaP products is that GSMaP_MVK contains a two-way (both forward and backward) morphing technique to propagate the rainy area from microwave radiometry. The GSMaP_Gauge dataset (available at ftp://rainmap@hokusai.eorc.jaxa.jp/standard_gauge/v5/hourly/) used in this study integrates the NOAA/CPC gauge-based analysis of global daily precipitation (Xie et al. 2007) into the GSMaP_MVK reanalysis version for realizing the satellite–gauge combination. Some literature highlights that the GSMaP products have been attractive to a wide range of weather forecasting and hydrologic applications owing to its superiority in spatiotemporal resolution (Tian et al. 2009; Ushio et al. 2009).

b. *Gauge datasets*

The ground gauge observations from four different data sources were herein used qualitatively in evaluating and validating the error of satellite precipitation estimates over the surrounding area of the Diaoyu Islands. These four reference datasets include the China Gauge-Based Daily Precipitation Analysis (CGDPA), the Asian Precipitation–Highly Resolved Observational Data Integration Toward Evaluation of Water Resources (APHRODITE) over land in Japan (APHRO_JP), Taiwan Daily Precipitation Observations (TDPO), and NOAA's Integrated Surface Database (ISD). Among them, CGDPA is the official daily gridded precipitation product (0.25° × 0.25°) released by National Meteorological Information Center (NMIC) of the China Meteorological Administration (CMA). This product, based on about 2400 gauge stations in China from 1955 to present, adopts an optimal interpolation (OI) method proposed by Xie et al. (2007) to rebuild the daily climatological precipitation field over mainland China (Shen and Xiong 2016). APHRO_JP is a gridded surface daily precipitation dataset starting from 1900 covering all of Japan with 0.05° × 0.05° grids except for some small islands (Kamiguchi et al. 2010). This product is derived from rain gauge data observed by JMA, and its spatial interpolation method considering precipitation climatology and topographical effect is developed by the Meteorological Research Institute (MRI). The

TABLE 1. Coverage and spatiotemporal resolutions of satellite-based precipitation products and ground-based observation data.

Product	Temporal resolution	Spatial resolution	Period	Coverage
Satellite precipitation				
TMPA-V7	3 hourly	0.25°	From 1 Jan 1998 to present	50°N–50°S
CMORPH-CRT	Daily	0.25°	From 1 Jan 1998 to 31 Dec 2013	60°N–60°S
PERSIANN-CDR	Daily	0.25°	From 1 Jan 1983 to present	60°N–60°S
GSMaP_Gauge	1 hourly	0.1°	From 1 Mar 2000 to 30 Nov 2010	60°N–60°S
Ground observations				
CGDPA	Daily	0.25°	From 1 Jan 1950 to present	Mainland China
APHRO_JP	Daily	0.05°	From 1 Jan 1900 to 31 Dec 2011	Mainland Japan
TDPO	Daily	Point scale	From 1 Jan 1981 to present	Taiwan region
ISD	Daily	Point scale	From 1 Jan 1900 to present	Global but incomplete

dataset is well quality controlled and thoroughly checked for errors and inconsistencies (Yatagai et al. 2012). Therefore, APHRO_JP can be expected to have rather good quality for mainland Japan. TDPO is a daily point-scale rainfall dataset collected from the standard weather observation network in Taiwan (http://www.cwb.gov.tw/V7e/climate/dailyPrecipitation/dP.htm). This rain gauge network is maintained by the Central Weather Bureau (CWB) of Taiwan. The available daily TDPO dataset spans the period from 1 January 1981 to the present. Last, ISD is a global surface observation dataset that merges numerous hourly gauge data into a common format and data model. It is the outcome of the Integrated Surface Database project initiated by NOAA's National Climatic Data Center (now the National Centers for Environmental Information), which contains the most common meteorological parameters (e.g., precipitation amounts for various time periods) from more than 20 000 stations worldwide (from 1900 to present). At present, there are more than 11 000 active stations that are updated daily in the database (Smith et al. 2011). In our study, CGDPA, APHRO_JP, and TDPO were used to evaluate the four chosen satellite precipitation estimates over the eastern coast of China, Japan, and Taiwan, respectively, and then the daily in situ observations on 12 islands extracted from ISD were used to further validate the accuracy of satellite retrievals over the surrounding seas adjacent to the Diaoyu Islands.

Table 1 shows the spatiotemporal resolutions and time coverage of all the satellite-based and ground-based rainfall datasets used in this paper. We can see that these eight different precipitation datasets have no standard data format and spatiotemporal resolution; therefore, the first step in processing was to convert them to a common resolution. Except for the pointed TDPO and ISD, all other gridded precipitation products were aggregated or resampled onto the daily, 0.25° × 0.25° resolution. In particular, to precisely match 3-hourly TMPA-V7 datasets to the daily estimates, the rainfall rates at 0000 and 2400 UTC were only aggregated 1.5 h for the current day while rainfall rates at other times (i.e., 0300, 0600, 0900, 1200, 1500, 1800, and 2100 UTC) were aggregated 3 h. Considering the limitation of the GSMaP_Gauge data availability (from 1 March 2000 to 30 November 2010), we selected an overlapping time span of the aforementioned precipitation datasets, a complete 9 years (2001–09), as the study period.

3. Results and analysis

a. Rainfall characteristics of the Diaoyu Islands

Figure 2 displays the spatial distributions of mean annual precipitation of four gauge-adjusted satellite precipitation estimates on the 0.25° × 0.25° resolution grid for the 9-yr study period. First, one can see that there is an apparent strip rain belt along the northeastern 45° direction of the island of Taiwan extending to the Japanese island of Kyushu. Physically, this rain belt should be associated with the Kuroshio from Taiwan to Japan, which is the strong north-flowing ocean current on the northwestern side of the North Pacific Ocean. The Kuroshio transports a huge amount of heat from the tropics to northern midlatitudes (Sawada and Handa 1998). The transported heat and moisture influence the regional atmospheric circulation by energizing storms, which anchors the major storm tracks along the Kuroshio path (O'Reilly and Czaja 2015). Figure 2 shows that the rain belt agrees well with the Kuroshio path in space. Interestingly, the Diaoyu Islands are almost located on the central axis line of this rain belt. In addition, we note that TMPA-V7, CMORPH-CRT, and GSMaP_Gauge generally have a similar distribution pattern, while the strip rain belt derived from PERSIANN-CDR seems to be broken off. This arises because the first three products all use the PMW observations with superior quality as a major source of input data as well as the IR data, but PERSIANN primarily relies on infrared

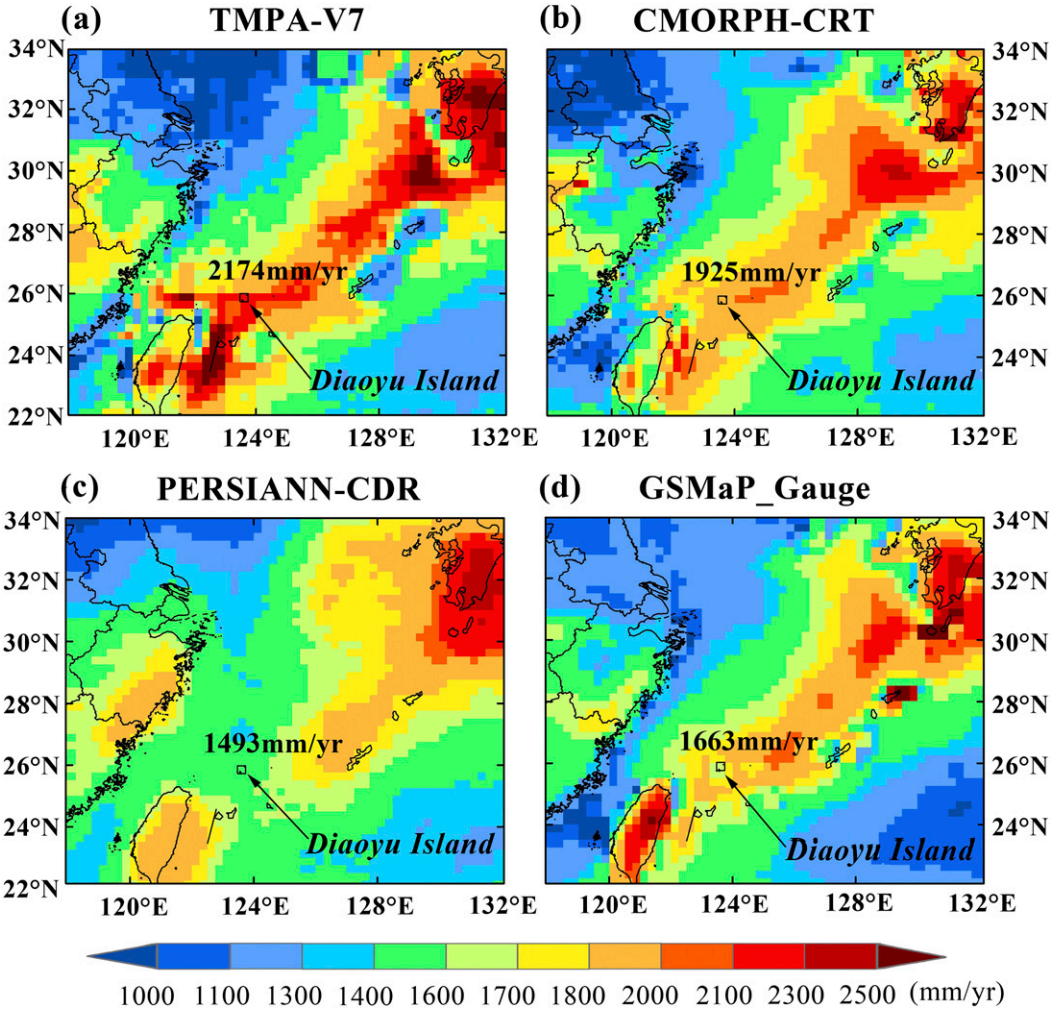

FIG. 2. Spatial distributions of mean annual precipitation of four satellite precipitation estimates in the study domain during the period of 2001–09.

information (Ashouri et al. 2015). Hence, it is quite plausible that there exists a significant difference in spatial pattern between PERSIANN-CDR and other products. It is worth noting that a more similar pattern was associated with CMORPH-CRT and GSMaP_Gauge, as they adopted the same Lagrangian time-interpolation scheme and morphing vector technique to merge the PWM and IR estimates. Relative to the average of annual precipitation of these four satellite-based products, the overestimation with TMPA-V7 was especially remarkable over the Diaoyu Islands and their adjacent sea, while PERSIANN-CDR had an evident underestimation. Over this rain belt, CMORPH-CRT and GSMaP_Gauge were closer to the average estimation. With respect to the Diaoyu Islands, the values of average annual rainfall are 2174 mm yr^{-1} for TMPA-V7, 1925 mm yr^{-1} for CMORPH-CRT, 1493 mm yr^{-1} for PERSIANN-CDR, and 1663 mm yr^{-1} for GSMaP_Gauge.

Figure 3 shows the intensity distribution of daily precipitation amount (Fig. 3a) and precipitation events (Fig. 3b) of these four products over the Diaoyu Islands. From Fig. 3a, we can see that the intensity distribution patterns of CMORPH-CRT and GSMaP_Gauge are quite similar, as are the spatial distribution patterns in Fig. 2. In practice, both of these two satellite products apply the motion vectors derived from half-hourly interval geostationary IR images to propagate the relatively high-quality precipitation estimates derived from PMW observations. During this process, the pattern and intensity of the precipitation features are modified by performing the same time-weighted linear interpolation in both forward and backward directions. Thus, the two morphing-based retrieval systems generate spatiotemporally

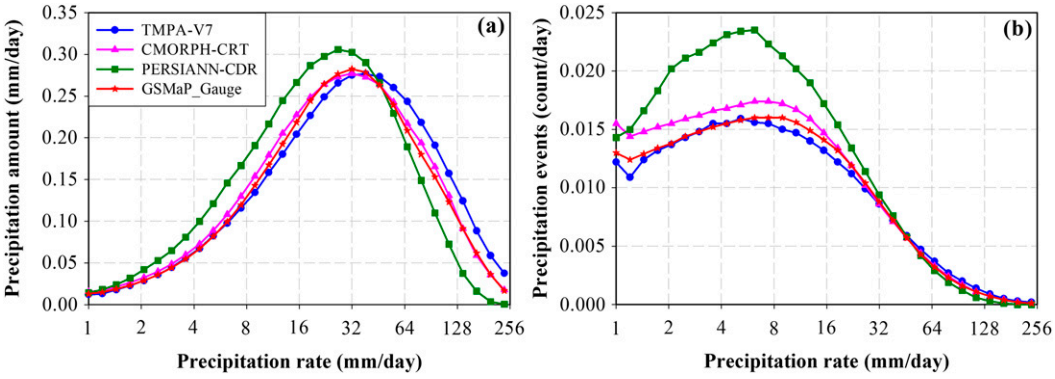

FIG. 3. Intensity distribution of (a) daily precipitation amount (mm day^{-1}) and (b) precipitation events (count per day) from the four satellite precipitation estimates at the Diaoyu Islands. The logarithmic scale was used to bin the precipitation rates.

consecutive microwave-derived precipitation estimates over the globe (Joyce et al. 2004; Kubota et al. 2007). The intensity distribution presented in Fig. 3a further confirms that there is little difference between CMORPH-CRT and GSMaP_Gauge in terms of the algorithm itself. Additionally, we found that the relative overestimation with TMPA-V7 primarily occurs at high rain rates of >50 mm day^{-1} (Fig. 3a). When compared to the other three algorithms, TMPA-V7 seems to be more prone to overestimate extreme precipitation events, such as typhoon storms. As for PERSIANN-CDR, it has an evident tendency to relatively underestimate higher rainfall rates and overestimate lower ones. Among the four satellite precipitation estimation algorithms, PERSIANN-CDR primarily relies on infrared information that the surface rainfall can be inferred from analyzing the cloud-top characteristics, that is, the cloud-top temperature. The obvious underestimation of PERSIANN-CDR at high rain rates is probably associated with the weak linkage between the cloud-top temperature and the convective storms during the summer months (Tuttle et al. 2008; Hamada et al. 2015). In contrast, the other three products (TMPA-V7, CMORPH-CRT, and GSMaP_Gauge) incorporated more passive microwave data, which have a more direct physical connection to the hydrometeors in the atmosphere. Therefore, they have a more similar distribution pattern of rainfall intensity. On the other hand, Fig. 3b illustrated that TMPA-V7, CMORPH-CRT, and GSMaP_Gauge have better agreement at low rain rates, while PERSIANN-CDR yields 20%–60% more rainy events than the other three products across the range of 2–16 mm day^{-1}. This could be chiefly attributed to the higher false detection in the IR retrievals. Relative to PMW, more no-raining areas may be mistaken as raining ones during the screening process of IR. Besides, such an intensity distribution feature of rainy events closely corresponds to PERSIANN-CDR's relative overestimation at low rain rates in Fig. 3a.

Since a whole year is involved in Fig. 3, we further investigate the seasonality of satellite precipitation estimates for a more insightful understanding. The intensity distribution of daily precipitation amount for each of the four seasons is shown in Fig. 4. Generally speaking, CMORPH-CRT and GSMaP_Gauge remain in good agreement with each other throughout all the seasons. In addition, one tends to see relatively larger differences between different products in spring and summer than in autumn and winter. Most notably, the severe underestimation with PERSIANN-CDR at high rain rates mainly occurs in the summer season. This result confirms the assertion of Tuttle et al. (2008) that the IR-based retrieval technique has an inherent deficiency that using IR brightness temperatures to estimate precipitation will yield a large error when the convective clouds, which frequently occur in summer, have a higher brightness temperature than the commonly used temperature threshold. This further supports our aforementioned analysis and explanation for the intensity distribution feature of PERSIANN-CDR as shown in Fig. 3.

b. *Comparison and validation of satellite precipitation estimates*

The purpose of the following section is to examine and compare the data accuracy of these four satellite-based estimates against the ground observations. The quantitative accuracy of satellite precipitation estimates was assessed using several representative statistical indices, including correlation coefficient (CC), root-mean-square error (RMSE), mean error (ME), mean absolute error (MAE), relative bias (BIAS), and contingency-table-based detection of rainy events [i.e., probability of detection (POD), false alarm rate (FAR), and critical

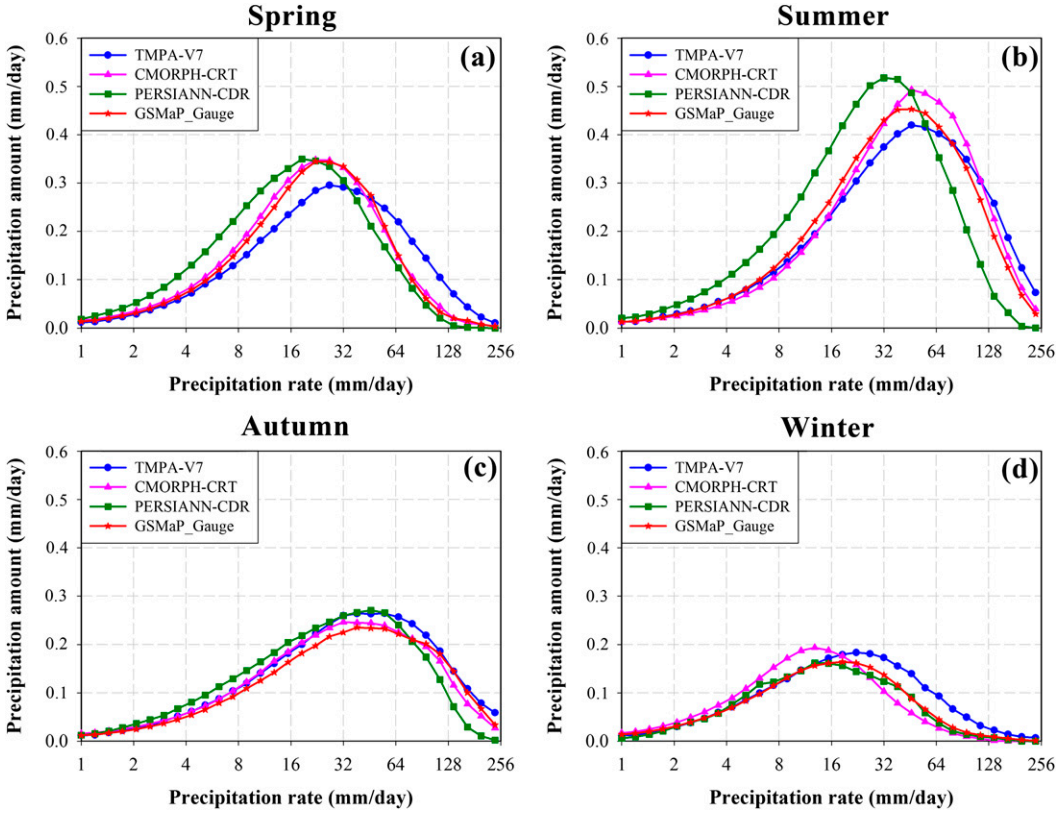

FIG. 4. As in Fig. 3a, but for the four seasons: (a) spring (March–May), (b) summer (June–August), (c) autumn (September–November), and (d) winter (December–February).

success index (CSI)]. A detailed description of these statistical indices is provided in Table 1 of Yong et al. (2010). In our study, we first employed two grid-based (i.e., CGDPA and APHRO_JP) and one gauge-based (TDPO) ground observation datasets to benchmark the four chosen satellite rainfall products over the eastern China, mainland Japan, and Taiwan regions, respectively. Figures 5 and 6 show the spatial distributions of CC and ME between satellite retrievals and gauge observations over eastern China and mainland Japan. It is clear that GSMaP_Gauge has higher correlation and lower error than others over both validation regions, while the poorest performance occurs in the PERSIANN-CDR with the lowest CC and largest ME values. As for CMORPH-CRT and TMPA-V7, the former generally looks better than the latter. Among the four studied satellite precipitation products, GSMaP_Gauge has the best performance, especially for its remarkable correlation with ground observations.

The daily TDPO data used in this study were gathered from the ground observation network in Taiwan, which is composed of 33 standard weather stations evenly distributed throughout all of Taiwan and its adjacent islands (see Fig. 7). Therefore, these observed stations are able to represent the rainfall characteristics over Taiwan and its surrounding seas to a fair extent. Scatterplots of daily comparison of four satellite precipitation estimates versus gauge observations are shown in Fig. 8. Similar to the evaluation results in eastern China and mainland Japan, statistics with GSMaP_Gauge are still better than those values obtained from the other three products. In contrast, PERSIANN-CDR with the lowest CC and largest RMSE has the poorest performance. Furthermore, the scatterplot of PERSIANN-CDR demonstrates a nonlinear exponential distribution, especially for the evident downward deviation at middle and higher rain rates (Fig. 8c). Such systematic negative biases seem to be much more serious than the other three products. Additionally, one tends to see the relatively slight differences that exist between CMORPH-CRT and TMPA-V7.

The daily statistical results in three different regions are summarized in Table 2. Almost all the statistical indices further manifest that GSMaP_Gauge outperformed the other three products with higher CC, lower RMSE and MAE, and better detection for rainy events (including POD, FAR, and CSI). Unusually, CMORPH-CRT and PERSIANN-CDR have slightly

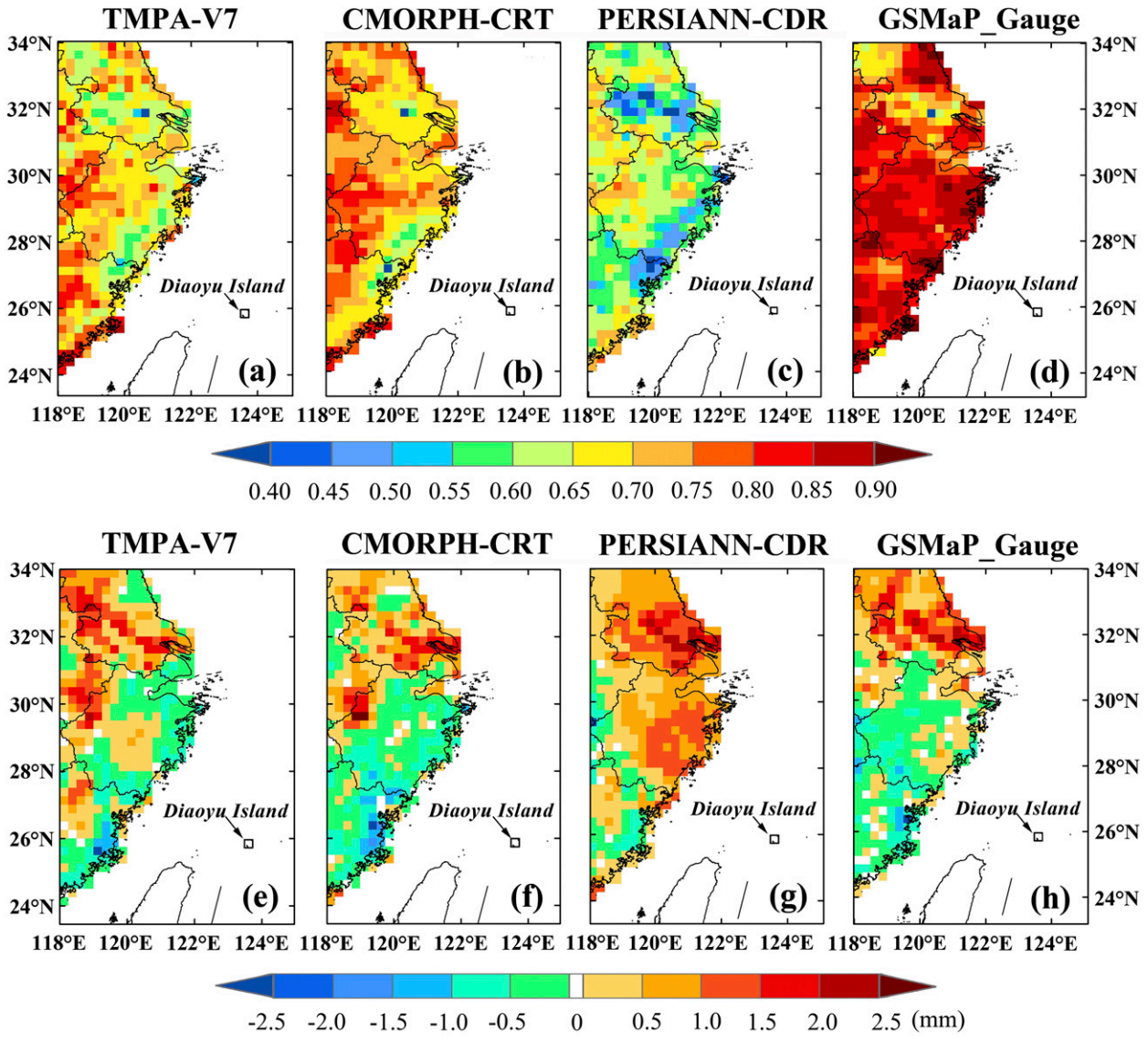

FIG. 5. Spatial distribution of statistical indices derived from the four satellite precipitation estimates vs gauge observations at daily, 0.25° × 0.25° resolution over eastern China: (a)–(d) CC and (e)–(h) ME.

lower BIAS and ME than GSMaP_Gauge over eastern China and mainland Japan, respectively, but their RMSE and MAE values are greater than those of GSMaP_Gauge. This phenomenon can be explained by the offset of positive and negative errors in the statistics for CMORPH-CRT and PERSIANN-CDR. Based on the similar evaluation results derived from three different validation regions, we can conclude that the GSMaP_Gauge algorithm is superior to the other three algorithms in estimating the land rainfall around the Diaoyu Islands. This could be attributed to two major reasons: 1) GSMaP_Gauge adopts the daily CPC data for the bias correction, which looks better than the monthly gauge analyses used in TMPA-V7 and PERSIANN-CDR; and 2) compared to CMORPH-CRT with the same daily CPC adjustments, GSMaP_Gauge employs two additional datasets (i.e., GANAL and MGDSST) for calculating lookup tables, which are referred by the GSMaP microwave imager and sounder algorithms. Because of the denser in situ data over East Asia involved, GSMaP_Gauge seems to have a relatively better performance over the surrounding counties and regions of the Diaoyu Islands.

To further validate the accuracy of the four satellite precipitation estimates over the water bodies adjacent to the Diaoyu Islands, the in situ observations distributed on 12 islands between Taiwan and Kyushu were extracted from the ISD (Fig. 9). Among this insular observation network, the gauge with number of 589740 belongs to

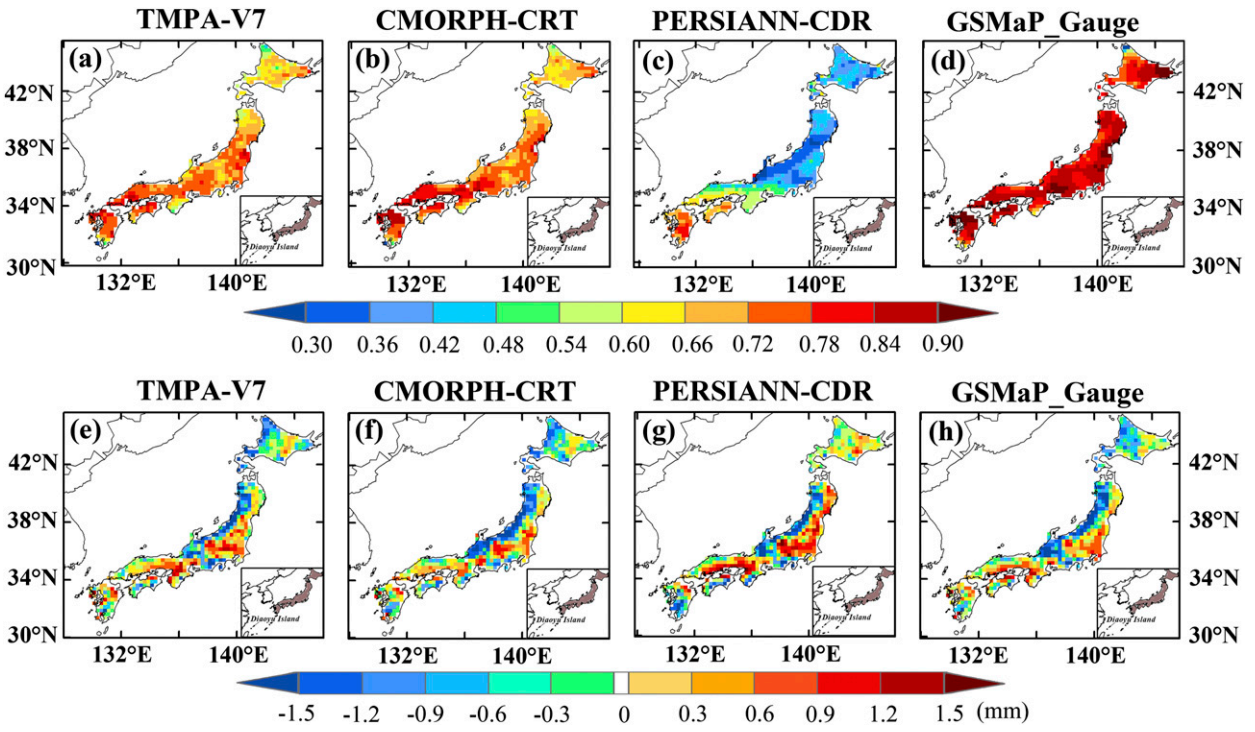

FIG. 6. As in Fig. 5, but for mainland Japan.

Taiwan and the other 11 gauges belong to Japan. The density-colored scatterplots drawn in Fig. 10 give a clear indication of how these four satellite-based precipitation estimates perform at the daily scale. Similar to Fig. 8c, PERSIANN-CDR significantly underestimates precipitation at higher rain rates. In contrast, TMPA-V7, CMORPH-CRT, and GSMaP_Gauge have a similar scatter distribution pattern and their points are clustered more closely to the 1:1 line than those of PERSIANN-CDR. By analyzing the statistical indices between these four products, one can see that GSMaP_Gauge still has the best performance with highest correlation and lowest error and bias, which further supports our aforementioned evaluation results. However, we also note that all the satellite precipitation estimates possess significantly less skill when compared to those over land in Table 2. Taking the best GSMaP_Gauge estimates, for example, its CC value decreases from 0.85 over Japan to 0.48 over selected islets and the RMSE increases from 5.34 to 16.80 mm. This phenomenon is highly likely caused by the problematic "coastal" identification and different relationship between brightness temperatures and surface rainfall over land and ocean (McCollum and Ferraro 2005). Specifically, the satellite field of view (FOV) varies from ~10 to ~100 km, depending on different frequencies and sensors. Therefore, those small islands cannot be fully resolved at such resolutions. That is, it is difficult to exactly pinpoint the coastal line because of the varying FOV size. In addition, the mixed land and ocean surface in one satellite FOV further complicates the rainfall retrieval algorithms over those islets because of the different brightness temperature–precipitation relationship over land and ocean. Over ocean, the primary information source is from the emission signature at low-frequency channels (e.g., 10 and 19 GHz), while the most prominent signature over land is the brightness temperature decrease at high frequencies (>85 GHz) caused by the scattering effects (Ferraro and Marks 1995; Kummerow et al. 2001; Kummerow et al. 2011; You and Liu 2012; You et al. 2015). The mixed signature sources (emission over ocean and scattering over land) lead to large uncertainties when converting TBs to precipitation rate. Several prior studies have documented that there are high measurement uncertainties along coastlines or island chains (e.g., Tian and Peters-Lidard 2010; Tang et al. 2014; Yong et al. 2015).

c. *Spatiotemporal analysis of typhoon rainfall*

Because of the quasi-global coverage with subdaily temporal resolution, the satellite rainfall estimates have proven useful in monitoring the evolution processes of typhoon rainfall over the ungauged oceans and islands (Rodgers et al. 2001; Lonfat et al. 2004; As-syakur et al. 2013; Prat and Nelson 2013). Thus, we particularly

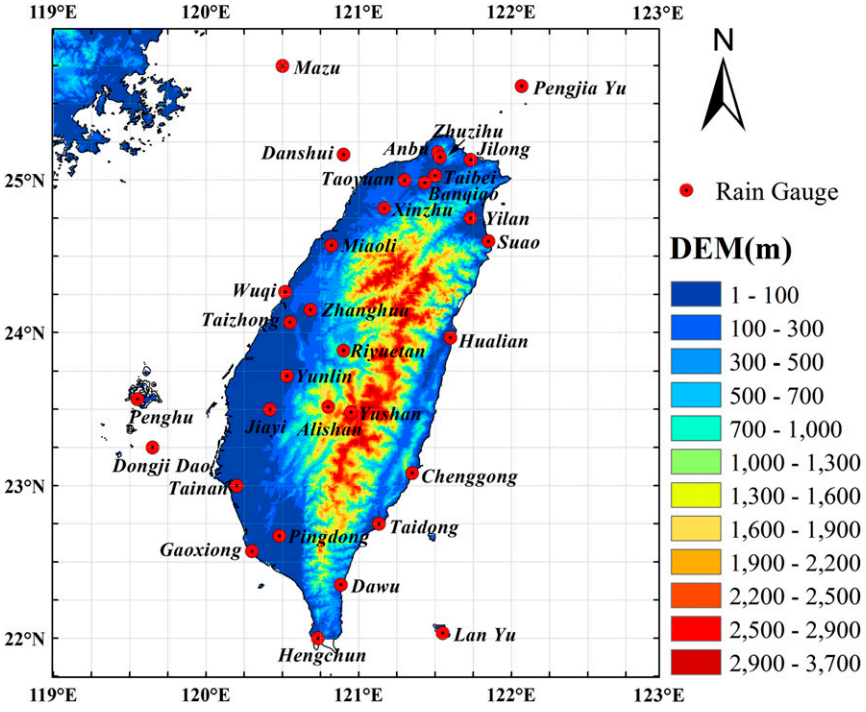

FIG. 7. Map of the 33 selected rain gauges in Taiwan for validating the satellite precipitation estimates.

focused on quantifying the typhoon rainfall and its contribution to local total rainfall over the Diaoyu Islands area by using the four aforementioned gauge-adjusted satellite products. Figure 11a displays the 67 typhoons passing through the study domain during the period from January 2001 to December 2009. The typhoon tracks were taken from the CMA Tropical Cyclone Data Center for the western North Pacific basin (http://tcdata.typhoon.gov.cn/en/index.html). Among the 67 typhoons, there are 24 supertyphoons with maximum average wind speed exceeding 51.0 m s^{-1}. During the period 2001–09, the Diaoyu Islands area experienced an average of 7.44 typhoons per year, ranging from 5 to 15 yr^{-1} (Fig. 11b). The maximum of 15 typhoons occurred in 2004. For this year, the strongest supertyphoon was Chaba, which caused a swath of damage from the Mariana Islands to Japan. The most severe damage occurred in Japan, where 18 people were killed and damages reached JPY 105.4 billion (959 million U.S. dollars). With respect to monthly statistics, typhoon activities were mostly concentrated over the summer months (July–September), accounting for about 70% of the whole year (Fig. 11c). Over the Diaoyu Islands area, almost no typhoons occurred in January–March. Looking further into the distributed characteristics of typhoon tracks, we found that these tracking lines seem to be denser over warmer waters in the south, while they became sparser toward the north as they veer over cooler waters. In terms of the largest typhoon event in each year, six out of nine supertyphoons for 2001–09 exhibit parallel tracks to the rainbelt direction and only three vertically passed through the rainbelt zone (refer to the colored directional lines in Fig. 11a). Thus, it is apparent that the northwestern Pacific typhoons brought a large amount of rainfall to this domain and constituted an important contribution to forming the strip rain belt from Taiwan to Japan.

Based on the four satellite-based precipitation estimates, we analyzed the time series variations of rainfall for the nine largest supertyphoons over the Diaoyu Islands (Fig. 12). Our analyses indicate that the subdaily TMPA-V7, CMORPH-CRT, and GSMaP_Gauge estimates generally demonstrated similar varying trends in tracking typhoon rainfall at the 3-hourly scale while demonstrating significant differences with PERSIANN-CDR. The daily PERSIANN-CDR estimates homogenize the highly variable rainstorm characteristics during typhoon events. Except for Typhoon Haitang of 2015, the rainfall duration of most typhoons over the Diaoyu Islands is no more than 48 h. So, we consider that the daily PERSIANN-CDR is not suitable for tracking the quick spatial and temporal evolution of typhoon rainfall, although it can provide a sufficiently long time series of precipitation that dates back to 1983. In terms of the rainfall characteristics, the maximum rainy event between 2001 and 2009 over the Diaoyu Islands came

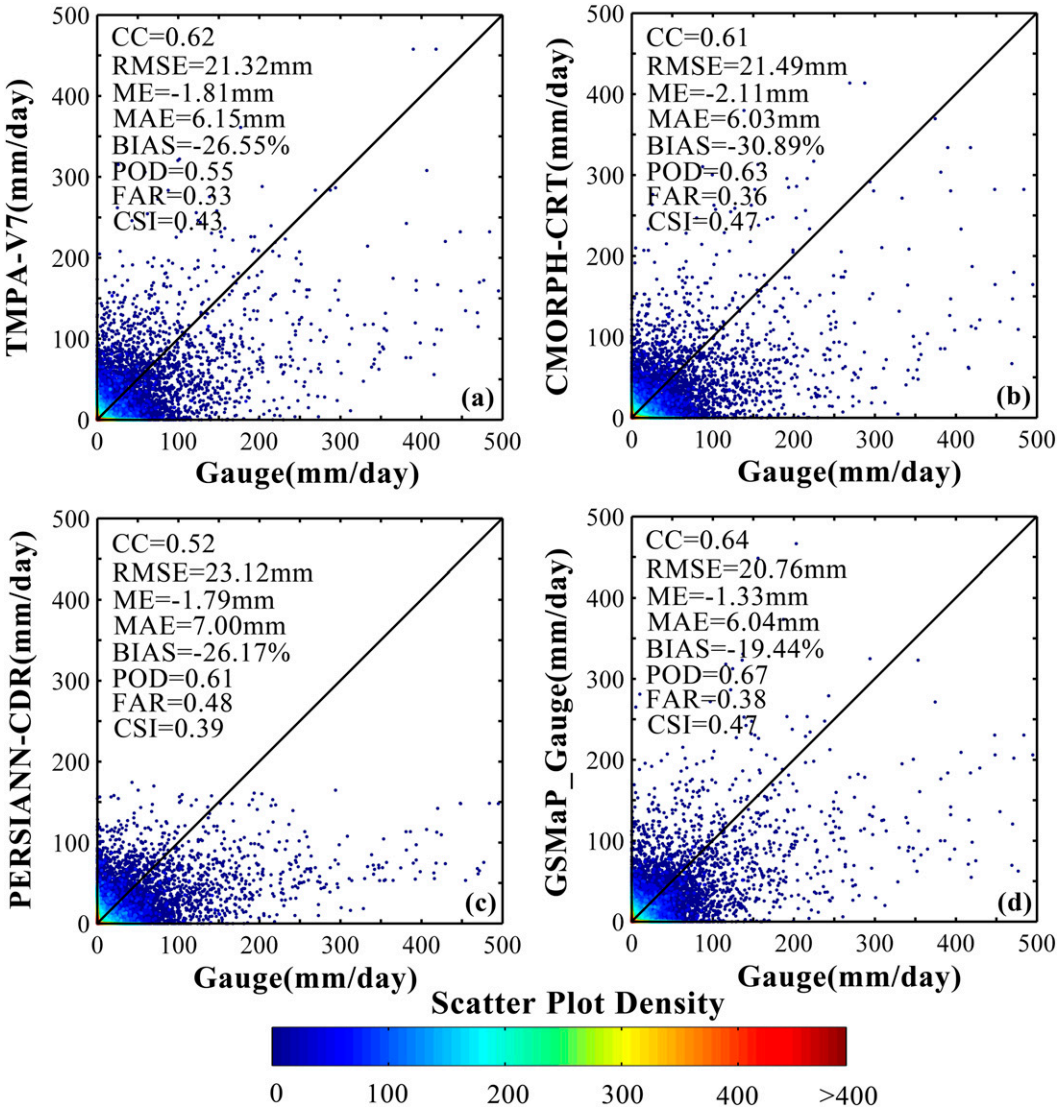

FIG. 8. Two-dimensional scatterplots of 9-yr average daily precipitation for (a) TMPA-V7, (b) CMORPH-CRT, (c) PERSIANN-CDR, and (d) GSMaP_Gauge against in situ observations from the 33 selected gauges in Fig. 7.

from Typhoon Chaba in 2004 and the minimum was Typhoon Rammasun in 2002. Moreover, we found that the typhoon rainfall of the Diaoyu Islands has a gradually increasing process in the early stages of each typhoon passage, which will take up approximately 60%–80% of the whole rainy duration. After the peak value arrival, the rainfall amount will then rapidly diminish. Normally, this disappearing process only lasts for several hours. This characteristic is specifically favorable to the early warning of typhoon storms.

Owing to the lack of accurate in situ observations on the Diaoyu Islands, we have to admit that uncertainties will inevitably exist in our following analysis of typhoon rainfall. But we believe that the common features derived from different satellite retrieval systems will be helpful to understand the typhoon rainfall characteristics of the ungauged Diaoyu Islands from a broader perspective. Meanwhile, the GSMaP_Gauge estimates with the best evaluation performance can also be regarded as the approximate reference of the true, areal rainfall of this area to a certain extent. Figures 13a–d show the spatial distributions of annual typhoon rainfall and Figs. 13e–h show its contribution to total rainfall computed from four satellite precipitation estimates over the study domain. With respect to the annual typhoon rainfall, all the satellite products demonstrate the similar distribution pattern (Figs. 13a–d). For this area, higher typhoon rainfall accumulations greater than 500 mm yr^{-1} were found over

TABLE 2. Statistical summary of four satellite precipitation estimates (TMPA-V7, CMORPH-CRT, PERSIANN-CDR, and GSMaP_Gauge) against ground observations over eastern China, mainland Japan, and Taiwan. Note that the boldface indicates the best statistics among four satellite precipitation estimates.

Products	CC	RMSE (mm)	ME (mm)	BIAS (%)	MAE (mm)	POD	FAR	CSI
China								
TMPA-V7	0.687	8.815	0.159	7.102	3.294	0.655	0.257	0.533
CMORPH-CRT	0.717	8.013	**0.046**	**4.427**	2.951	0.740	0.264	0.583
PERSIANN-CDR	0.554	9.287	0.595	19.631	4.229	0.765	0.495	0.434
GSMaP_Gauge	**0.818**	**6.243**	0.117	7.423	**2.410**	**0.810**	**0.252**	**0.634**
Japan								
TMPA-V7	0.700	8.238	−0.522	−10.040	3.714	0.521	0.197	0.455
CMORPH-CRT	0.726	7.162	−1.008	−20.480	3.353	0.529	0.186	0.463
PERSIANN-CDR	0.422	9.109	**−0.080**	**2.141**	4.966	**0.711**	0.425	0.463
GSMaP_Gauge	**0.844**	**5.337**	−0.634	−12.371	**2.533**	0.687	**0.152**	**0.607**
Taiwan								
TMPA-V7	0.619	21.320	−1.814	−26.552	6.145	0.549	**0.329**	0.433
CMORPH-CRT	0.610	21.486	−2.110	−30.891	**6.026**	0.634	0.358	0.469
PERSIANN-CDR	0.520	23.116	−1.787	−26.172	6.998	0.610	0.475	0.393
GSMaP_Gauge	**0.640**	**20.761**	**−1.328**	**−19.443**	6.039	**0.665**	0.382	**0.471**

southern Japan, Taiwan, and the southeastern sea area of the Diaoyu Islands. The rainfall accumulations between 300 and 500 mm yr^{-1} were found over the rainbelt zone starting from the waters near the Diaoyu Islands along the northeastern 45° direction extending to Kyushu. As for the Diaoyu Islands, the typhoon rainfall was approximately 530 mm yr^{-1} (refer to the GSMaP_Gauge estimates in Fig. 13d). Overall, the spatial distribution of typhoon rainfall is consistent with that of average annual precipitation in Fig. 11a. This implies that the typhoon rainfall has an important contribution to the total annual precipitation amounts, especially over the Kuroshio path. The spatial distribution of typhoon contribution was presented in Figs. 13e and 13f, which clearly shows that the relatively larger values corresponded to locations with the higher typhoon rainfall. Contribution ratio of about 30% was found for the Diaoyu Islands. Generally, it can be concluded that the northwestern Pacific typhoons brought higher rainfall

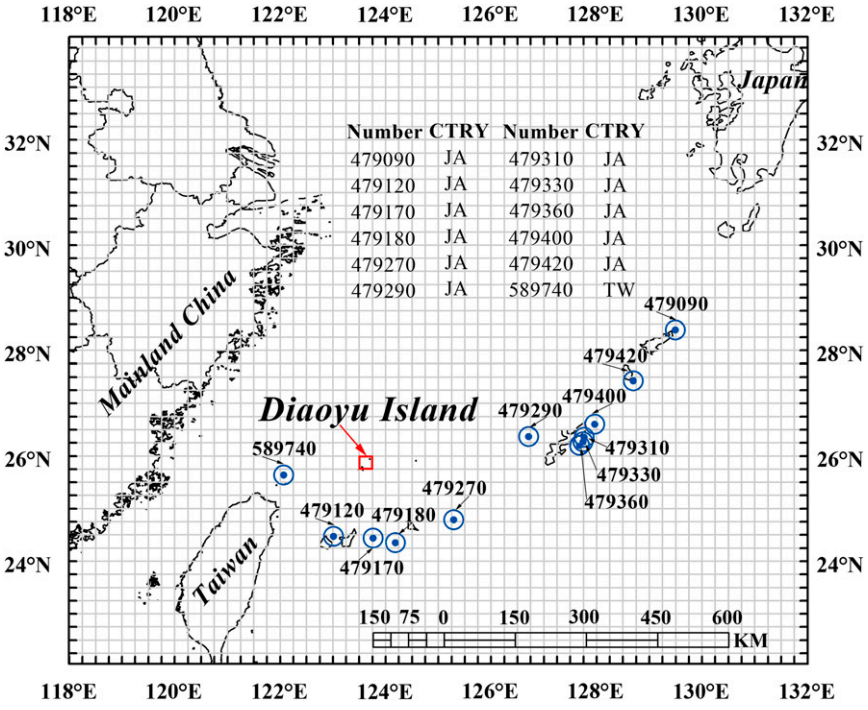

FIG. 9. Map of the 12 selected rain gauges on the islands for validating the satellite precipitation estimates over the adjacent sea to the Diaoyu Islands. CTRY represents Country, JA represents Japan, and TW represents Taiwan. Numbers are station IDs.

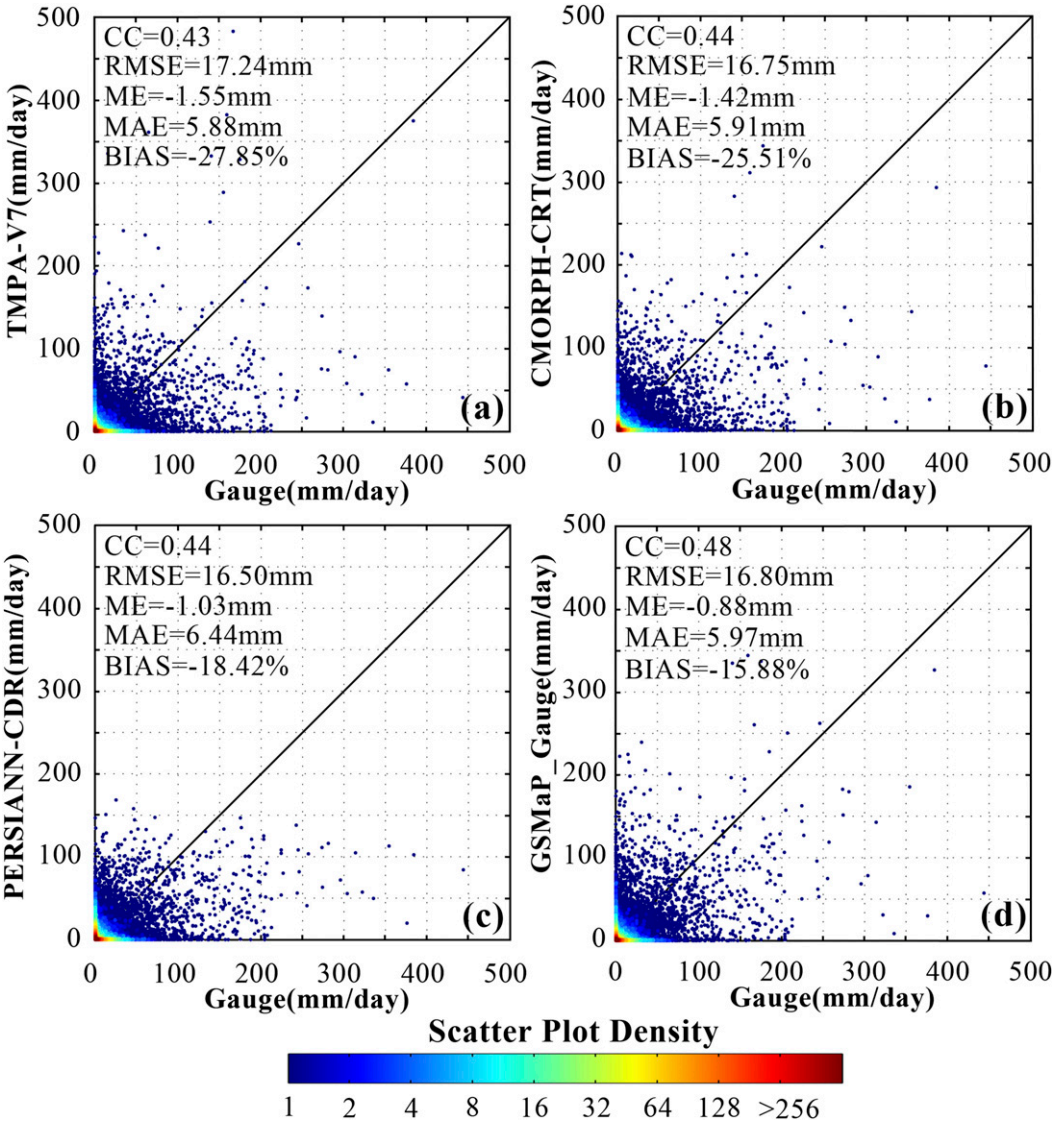

FIG. 10. Two-dimensional scatterplots of 9-yr average daily precipitation for (a) TMPA-V7, (b) CMORPH-CRT, (c) PERSIANN-CDR, and (d) GSMaP_Gauge against in situ observations from the 12 selected islets in Fig. 9.

contribution over the southern warmer waters of the area, while the northern cooler water presented less contribution. This feature is consistent with the analysis results of global tropical cyclones in Mendelsohn et al. (2012).

Finally, Fig. 14 depicts the annual typhoon accumulation (Fig. 14a) and typhoon rainfall ratio (Fig. 14b) on average for the whole study domain around the Diaoyu Islands. On a year-to-year basis, the typhoon rainfall derived from the four satellite precipitation estimates presented the better consistency and this domain experienced the average typhoon rain of 360 mm yr^{-1} during the 9-yr period, ranging from 260 mm yr^{-1} in 2009 to 570 mm yr^{-1} in 2004. Correspondingly, the minimum, mean, and maximum annual typhoon contributions were approximately 18%, 23%, and 36%, respectively. The largest typhoon rainfall and contribution ratio was in 2004, when together 15 large typhoon events and more tropical storms and tropical depressions crossed this domain. The most powerful supertyphoon, Typhoon Chaba, produced destructive winds and torrential rain. Heavy rain from Chaba severely impacted all the islands within this domain for about 53 h, with the Diaoyu Islands receiving over 235 mm of rain.

4. Conclusions and recommendations

In this study, four gauge-adjusted satellite precipitation estimates (TMPA-V7, CMORPH-CRT, PERSIANN-CDR, and GSMaP_Gauge) were systematically evaluated

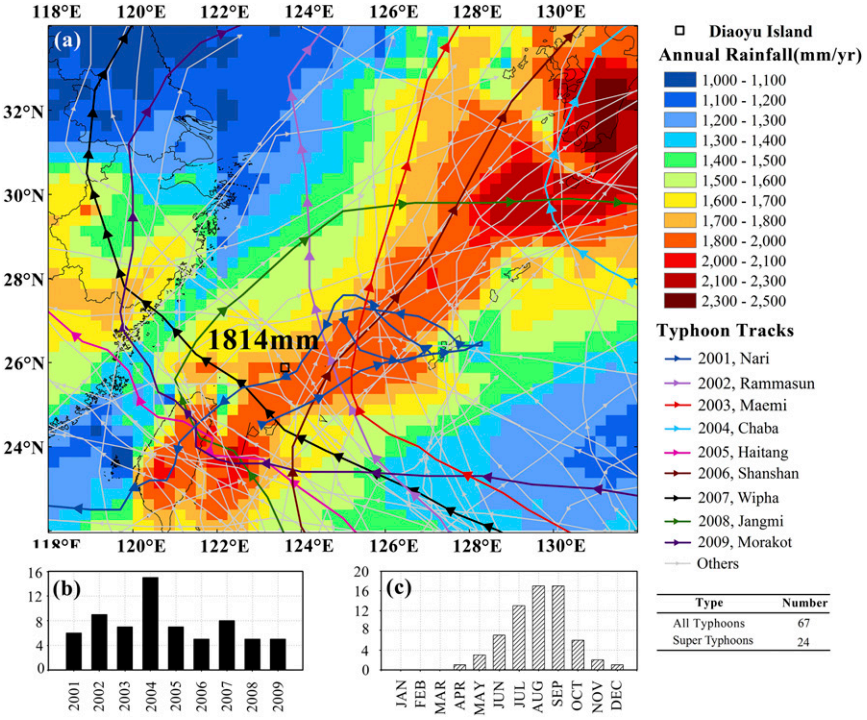

FIG. 11. (a) Typhoon tracks on background of average of annual accumulations of four satellite precipitation estimates, (b) annual number of typhoons, and (c) accumulative monthly number of typhoons during the period 2001–09 for our study domain.

for detecting the rainfall characteristics of the Diaoyu Islands area, with a particular focus on typhoon contribution. The main findings of this study can be summarized as follows.

1) When aggregated to annual scale, TMPA-V7, CMORPH-CRT, and GSMaP_Gauge presented a similar spatial distribution of rainfall amount over the study domain, while relatively large underestimation

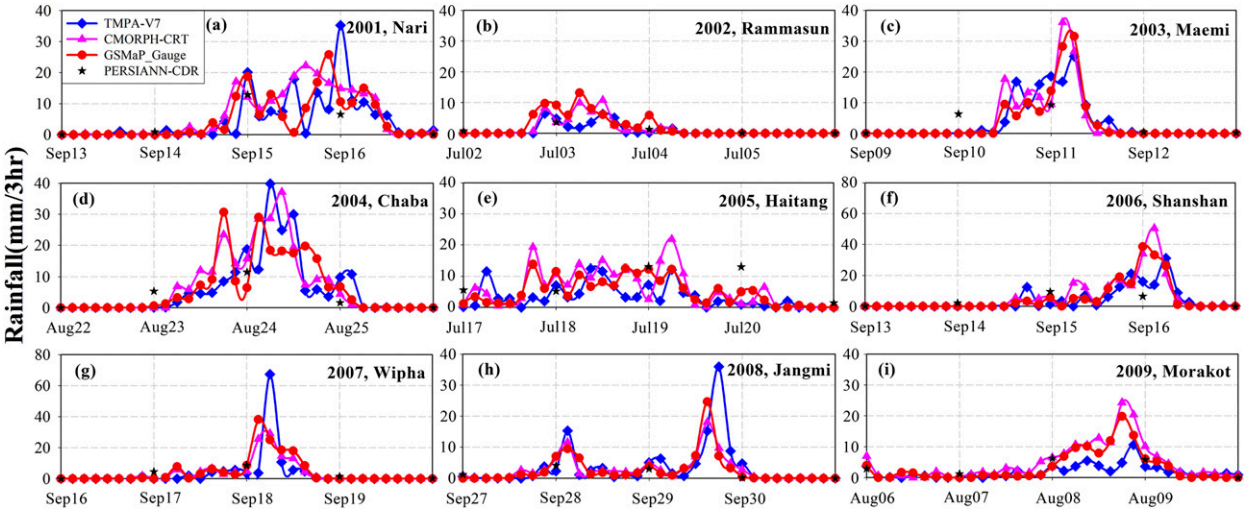

FIG. 12. Time series variations of the largest typhoon rainfall in each year over the Diaoyu Islands during the period 2001–09: (a) Nari, 2001; (b) Rammasun, 2002; (c) Maemi, 2003; (d) Chaba, 2004; (e) Haitang, 2005; (f) Shanshan, 2006; (g) Wipha, 2007; (h) Jangmi, 2008; and (i) Morakot, 2009. Note that the subdaily TMPA-V7, CMORPH-CRT, and GSMaP_Gauge datasets are displayed at 3-hourly scale, but PERSIANN-CDR only offers the daily rainfall estimates.

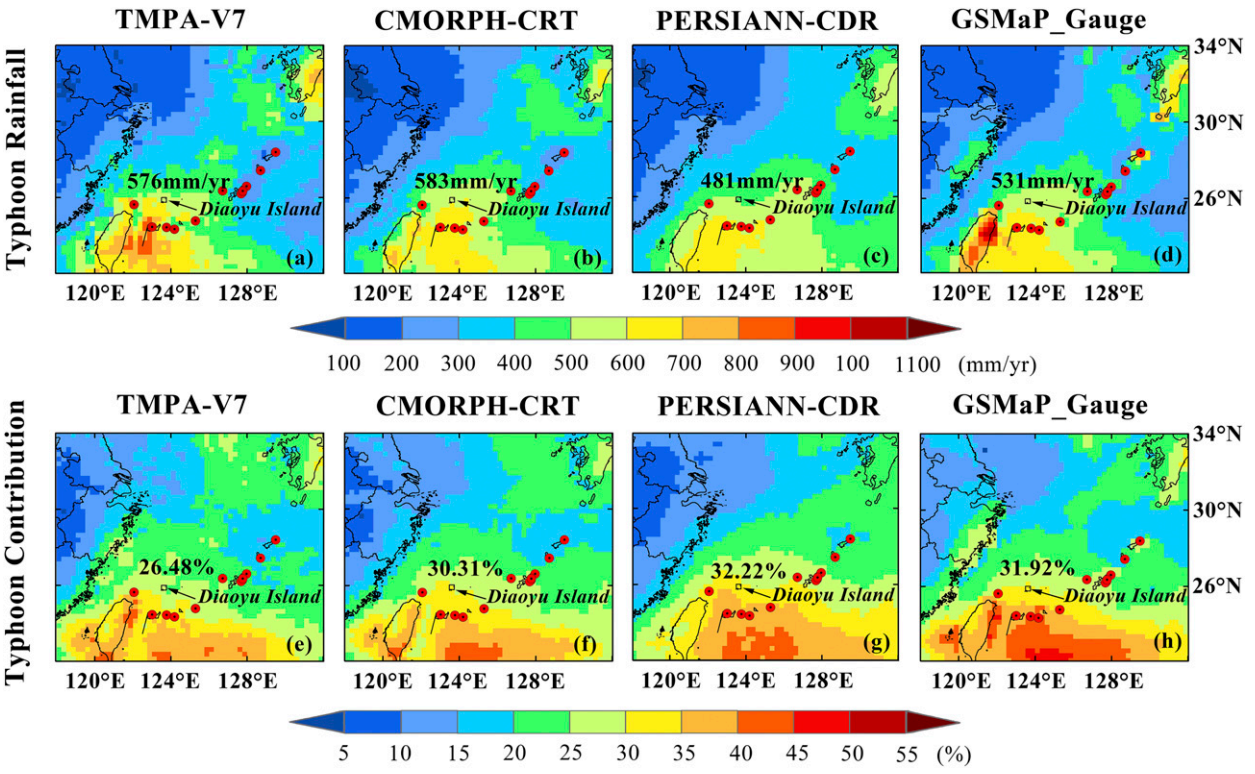

FIG. 13. Spatial distribution of (a)–(d) typhoon rainfall (mm yr^{-1}) and (e)–(h) typhoon contribution (%) computed from the four satellite precipitation estimates for 2001–09 over the study domain.

was found for PERSIANN-CDR. On daily time scales, CMORPH-CRT and GSMaP_Gauge tend to have the closest performance of intensity distribution because the same Lagrangian time-interpolation scheme and morphing vector technique were employed to merge the PWM and IR estimates in their retrieval systems. In contrast, PERSIANN-CDR exhibits significant overestimation at lower rain rates and underestimation at

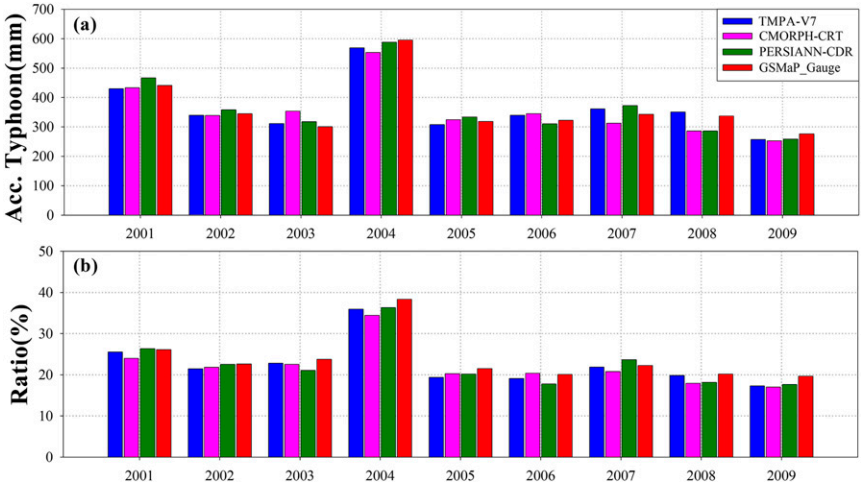

FIG. 14. (a) Yearly typhoon rainfall accumulation and (b) typhoon contribution for the annual precipitation budget computed from the four satellite precipitation estimates for the study domain. Note that typhoon rainfall amounts were normalized with respect to the study domain impacted by all typhoon events for a given year.

higher ones. Because of the subdaily temporal resolution, TMPA-V7, CMORPH-CRT, and GSMaP_Gauge successfully capture the rapid evolution processes of typhoon rainfall over this area, while the daily PERSIANN-CDR seems unsuitable to track the typhoon rainfall variability.

2) When compared to ground-based measurements over eastern China, Japan, and 12 island in situ observations, GSMaP_Gauge shows the best rainfall estimates with the highest correlation and lowest error and bias, while PERSIANN-CDR has relatively worse performance. This is likely because the incorporation of denser in situ data over East Asia in GSMaP_Gauge effectively reduces the systematic biases of satellite retrieval, while the input data sources of PERSIANN-CDR primarily come from the infrared information with sparse gauge adjustment. As for the other two products, CMORPH-CRT correlates slightly better with observed rainfall than TMPA-V7 and with relatively lower RMSE and MAE. Based on the above analyses, we recommend using the hourly GSMaP_Gauge estimates to detect and quantify the typhoon rainfall characteristics over the East Asia area.
3) Satellite-based estimates indicate an apparent strip of rain belt along the northeastern 45° direction of the island of Taiwan extending to the Japanese island of Kyushu. This rain belt is physically associated with the Kuroshio, which influences the tracks of the northwestern Pacific tropical cyclones. The typhoon storms carrying abundant rainfall frequently passed the Kuroshio path (about 7–8 typhoon events per year) and constitute an important contribution to forming this rain belt. The most typhoons occurred in summer (July–September), accounting for about 70% of the whole year. It is also noteworthy that higher contribution ratio of typhoon rainfall was found over the southern part of the Diaoyu Islands, while the northern area presented less typhoon contribution. In practice, the northwestern Pacific tropical cyclones are most intense over warm waters near the equator, and they will gradually lose their intensity toward the poles as the typhoon storms veer over cooler northern waters.
4) In terms of the Diaoyu Islands, the average values of annual typhoon rainfall and typhoon contribution for 2001–09 are approximately 530 mm yr^{-1} and 30%, respectively. The highest values were found for 2004. In this typhoon-intense year (with 15 typhoons crossing this area), the most powerful supertyphoon, Typhoon Chaba, brought total rainfall accumulation of 235 mm within 53 h on the Diaoyu Islands and led to severe property damages and human casualties for Japan. Because of the specific geographic location, the Diaoyu Islands play an important role for monitoring and forecasting the hydrometeorological hazards over this region.

In summary, this study demonstrated that there is a great potential in the use of satellite precipitation estimates in areas where ground observations are sparse or completely missing. Although the ground-based validation in this paper is limited to the surrounding counties and regions of the Diaoyu Islands, we considered that the assessment presented here can offer a valuable reference for understanding the local rainfall characteristics. Looking into the future, we believe that the ongoing GPM will substantially improve the capacity for monitoring and predicting the tropical cyclone structure and evolution through more accurate and more frequent precipitation measurements from space, aiming for a 0.5-h interval for the merging multisatellite observations (Huffman et al. 2015). This should help meteorologists and hydrologists to better understand how the hydrological cycle works over the ungauged regions of the globe.

Acknowledgments. This work was financially supported by National Natural Science Foundation of China (91547101, 51379056, and 91437214). Also, this work is partially sponsored by the 111 Project (B08048) and Open Fund of State Key Laboratory of Satellite Ocean Environment Dynamics, Second Institute of Oceanography (SOED1601). The authors thank three anonymous reviewers who helped to improve the earlier version of this paper.

REFERENCES

Aonashi, K., and Coauthors, 2009: GSMaP passive microwave precipitation retrieval algorithm: Algorithm description and validation. *J. Meteor. Soc. Japan*, **87A**, 119–136, doi:10.2151/jmsj.87A.119.

Ashouri, H., K.-L. Hsu, S. Sorooshian, D. K. Braithwaite, K. R. Knapp, L. D. Cecil, B. R. Nelson, and O. P. Prat, 2015: PERSIANN-CDR: Daily precipitation climate data record from multisatellite observations for hydrological and climate studies. *Bull. Amer. Meteor. Soc.*, **96**, 69–83, doi:10.1175/BAMS-D-13-00068.1.

As-syakur, A. R., T. Tanaka, T. Osawa, and M. S. Mahendra, 2013: Indonesian rainfall variability observation using TRMM multi-satellite data. *Int. J. Remote Sens.*, **34**, 7723–7738, doi:10.1080/01431161.2013.826837.

Behrangi, A., B. Khakbaz, T. C. Jaw, A. AghaKouchak, K. Hsu, and S. Sorooshian, 2011: Hydrologic evaluation of satellite precipitation products over a mid-size basin. *J. Hydrol.*, **397**, 225–237, doi:10.1016/j.jhydrol.2010.11.043.

Bitew, M. M., and M. Gebremichael, 2011: Evaluation of satellite rainfall products through hydrologic simulation in a fully distributed hydrologic model. *Water Resour. Res.*, **47**, W06526, doi:10.1029/2010WR009917.

——, ——, L. T. Ghebremichael, and Y. A. Bayissa, 2012: Evaluation of high-resolution satellite rainfall products through streamflow simulation in a hydrological modeling of a small mountainous watershed in Ethiopia. *J. Hydrometeor.*, **13**, 338–350, doi:10.1175/2011JHM1292.1.

Bowman, K. P., and M. D. Fowler, 2015: The diurnal cycle of precipitation in tropical cyclones. *J. Climate*, **28**, 5325–5334, doi:10.1175/JCLI-D-14-00804.1.

Chen, S., and Coauthors, 2013a: Similarity and difference of the two successive V6 and V7 TRMM multisatellite precipitation analysis performance over China. *J. Geophys. Res. Atmos.*, **118**, 13 060–13 074, doi:10.1002/2013JD019964.

——, and Coauthors, 2013b: Evaluation of the successive V6 and V7 TRMM multisatellite precipitation analysis over the continental United States. *Water Resour. Res.*, **49**, 8174–8186, doi:10.1002/2012WR012795.

Dare, R. E., N. E. Davidson, and J. L. McBride, 2012: Tropical cyclone contribution to rainfall over Australia. *Mon. Wea. Rev.*, **140**, 3606–3619, doi:10.1175/MWR-D-11-00340.1.

Ferraro, R., and G. Marks, 1995: The development of SSM/I rain rate retrieval algorithms using ground-based radar measurements. *J. Atmos. Oceanic Technol.*, **12**, 755–770, doi:10.1175/1520-0426(1995)012<0755:TDOSRR>2.0.CO;2.

Habib, E., A. Henschke, and R. F. Adler, 2009: Evaluation of TMPA satellite-based research and real-time rainfall estimates during six tropical-related heavy rainfall events over Louisiana, USA. *Atmos. Res.*, **94**, 373–388, doi:10.1016/j.atmosres.2009.06.015.

Hamada, A., Y. Tkayahu, C. Liu, and E. Zipser, 2015: Weak linkage between the heaviest rainfall and tallest storms. *Nat. Commun.*, **6**, 6213, doi:10.1038/ncomms7213.

Hou, A. Y., and Coauthors, 2014: The Global Precipitation Measurement Mission. *Bull. Amer. Meteor. Soc.*, **95**, 701–722, doi:10.1175/BAMS-D-13-00164.1.

Hsu, K. L., X. Gao, S. Sorooshian, and H. V. Gupta, 1997: Precipitation Estimation from Remotely Sensed Information using Artificial Neural Networks. *J. Appl. Meteor.*, **36**, 1176–1190, doi:10.1175/1520-0450(1997)036<1176:PEFRSI>2.0.CO;2.

Huffman, G. J., and D. T. Bolvin, 2015: Real-time TRMM Multi-Satellite Precipitation Analysis data set documentation. TRMM Rep., 48 pp. [Available online at ftp://trmmopen.gsfc.nasa.gov/pub/merged/V7Documents.]

——, and Coauthors, 2007: The TRMM Multisatellite Precipitation Analysis (TMPA): Quasi-global, multiyear, combined-sensor precipitation estimates at fine scales. *J. Hydrometeor.*, **8**, 38–55, doi:10.1175/JHM560.1.

——, R. F. Adler, D. T. Bolvin, and G. Gu, 2009: Improving the global precipitation record: GPCP version 2.1. *Geophys. Res. Lett.*, **36**, L17808, doi:10.1029/2009GL040000.

——, D. T. Bolvin, and E. J. Nelkin, 2015: Integrated Multi-satellitE Retrievals for GPM (IMERG) Technical Documentation. NASA/GSFC Code 612 Tech. Doc., 48 pp. [Available online at http://pmm.nasa.gov/sites/default/files/document_files/IMERG_doc.pdf.]

Joyce, R. J., J. E. Janowiak, P. A. Arkin, and P. Xie, 2004: CMORPH: A method that products global precipitation estimates from passive microwave and infrared data at high spatial and temporal resolution. *J. Hydrometeor.*, **5**, 487–503, doi:10.1175/1525-7541(2004)005<0487:CAMTPG>2.0.CO;2.

Kamiguchi, K., O. Arakawa, A. Kitoh, A. Yatagai, A. Hamada, and N. Yasutomi, 2010: Development of APHRO_JP, the first Japanese high-resolution daily precipitation product for more than 100 years. *Hydrol. Res. Lett.*, **4**, 60–64, doi:10.3178/hrl.4.60.

Khan, S. I., and Coauthors, 2012: Microwave satellite data for hydrologic modeling in ungauged basins. *IEEE Geosci. Remote Sens.*, **9**, 663–667, doi:10.1109/LGRS.2011.2177807.

Kubota, T., S. Shige, H. Hashizume, T. Ushio, K. Aonashi, M. Kachi, and K. Okamoto, 2007: Global precipitation map using satelliteborne microwave radiometers by the GSMaP project: Production and validation. *IEEE Trans. Geosci. Remote Sens.*, **45**, 2259–2275, doi:10.1109/TGRS.2007.895337.

Kummerow, C. D., and Coauthors, 2001: The evolution of the Goddard profiling algorithm (GPROF) for rainfall estimation from passive microwave sensors. *J. Appl. Meteor.*, **40**, 1801–1820, doi:10.1175/1520-0450(2001)040<1801:TEOTGP>2.0.CO;2.

——, S. Ringerud, J. Crook, D. Randel, and W. Berg, 2011: An observationally generated a priori database for microwave rainfall retrievals. *J. Atmos. Oceanic Technol.*, **28**, 113–130, doi:10.1175/2010JTECHA1468.1.

Lonfat, M., F. Marks, and S. Chen, 2004: Precipitation distribution in tropical cyclones using the Tropical Rainfall Measuring Mission (TRMM) Microwave Imager: A global perspective. *Mon. Wea. Rev.*, **132**, 1645–1660, doi:10.1175/1520-0493(2004)132<1645:PDITCU>2.0.CO;2.

McCollum, J. R., and R. Ferraro, 2005: Microwave rainfall estimation over coasts. *J. Atmos. Oceanic Technol.*, **22**, 497–512, doi:10.1175/JTECH1732.1.

——, W. F. Krajewshi, R. Ferraro, and M. B. Ba, 2002: Evaluation of biases of satellite rainfall estimation algorithms over the continental United States. *J. Appl. Meteor.*, **41**, 1065–1080, doi:10.1175/1520-0450(2002)041<1065:EOBOSR>2.0.CO;2.

Mendelsohn, R., K. Emanuel, S. Chonabayashi, and L. Bakkensen, 2012: The impact of climate change on global tropical cyclone damage. *Nat. Climate Change*, **2**, 205–209, doi:10.1038/nclimate1357.

Nogueira, R. C., and B. D. Kleim, 2011: Contributions of Atlantic tropical cyclones to monthly and seasonal rainfall in the eastern United States 1960–2007. *Theor. Appl. Climatol.*, **103**, 213–227, doi:10.1007/s00704-010-0292-9.

Okamoto, K., N. Takahashi, K. Iwanami, S. Shige, and T. Kubota, 2008: High precision and high resolution global precipitation map from satellite data. *Proc. MICRORAD 2008*, Florence, Italy, IEEE, 1–4, doi:10.1109/MICRAD.2008.4579485.

O'Reilly, C. H., and A. Czaja, 2015: The response of the Pacific storm track and atmospheric circulation to Kuroshio Extension variability. *Quart. J. Roy. Meteor. Soc.*, **141**, 52–66, doi:10.1002/qj.2334.

Prat, O. P., and B. R. Nelson, 2013: Mapping the world's tropical cyclone rainfall contribution over land using the TRMM Multi-satellite Precipitation Analysis. *Water Resour. Res.*, **49**, 7236–7254, doi:10.1002/wrcr.20527.

Rodgers, E. B., R. F. Adler, and H. F. Pierce, 2001: Contribution of tropical cyclones to the North Atlantic climatological rainfall as observed from satellite. *J. Appl. Meteor.*, **40**, 1785–1800, doi:10.1175/1520-0450(2001)040<1785:COTCTT>2.0.CO;2.

Romilly, T. G., and M. Gebremichael, 2011: Evaluation of satellite rainfall estimates over Ethiopian river basins. *Hydrol. Earth Syst. Sci.*, **15**, 1505–1514, doi:10.5194/hess-15-1505-2011.

Sawada, K., and N. Handa, 1998: Variability of the path of the Kuroshio ocean current over the past 25,000 years. *Nature*, **392**, 592–595, doi:10.1038/33391.

Shen, Y., and A. Xiong, 2016: Validation and comparison of a new gauge-based precipitation analysis over mainland China. *Int. J. Climatol.*, **36**, 252–265, doi:10.1002/joc.4341.

——, ——, Y. Wang, and P. Xie, 2010: Performance of high-resolution satellite precipitation products over China. *J. Geophys. Res.*, **115**, D02114, doi:10.1029/2009JD012097.

Smith, A., N. Lott, and R. Vose, 2011: The Integrated Surface Database: Recent developments and partnerships. *Bull. Amer. Meteor. Soc.*, **92**, 704–708, doi:10.1175/2011BAMS3015.1.

Sorooshian, S., K. L. Hsu, X. Gao, H. V. Gupta, B. Imam, and D. Braithwaite, 2000: Evaluation of PERSIANN system satellite-based estimates of tropical rainfall. *Bull. Amer. Meteor. Soc.*, **81**, 2035–2046, doi:10.1175/1520-0477(2000)081<2035:EOPSSE>2.3.CO;2.

Stisen, S., and I. Sandholt, 2010: Evaluation of remote-sensing-based rainfall products through predictive capability in hydrological runoff modeling. *Hydrol. Processes*, **24**, 879–891, doi:10.1002/hyp.7529.

Su, F., Y. Hong, and D. P. Lettenmaier, 2008: Evaluation of TRMM Multisatellite Precipitation Analysis (TMPA) and its utility in hydrologic prediction in the La Plata basin. *J. Hydrometeor.*, **9**, 622–640, doi:10.1175/2007JHM944.1.

Tang, L., Y. Tian, and X. Lin, 2014: Validation of precipitation retrievals from satellite-based passive microwave sensors. *J. Geophys. Res. Atmos.*, **119**, 4546–4567, doi:10.1002/2013JD020933.

Tapiador, F. J., and Coauthors, 2012: Global precipitation measurement: Methods, datasets and applications. *Atmos. Res.*, **104–105**, 70–97, doi:10.1016/j.atmosres.2011.10.021.

Tian, Y., and Coauthors, 2009: Component analysis of errors in satellite-based precipitation estimates. *J. Geophys. Res.*, **114**, D24101, doi:10.1029/2009JD011949.

——, and C. D. Peters-Lidard, 2010: A global map of uncertainties in satellite-based precipitation measurements. *Geophys. Res. Lett.*, **37**, L24407, doi:10.1029/2010GL046008.

Tobin, K. J., and M. E. Bennett, 2010: Adjusting satellite precipitation data to facilitate hydrologic modeling. *J. Hydrometeor.*, **11**, 966–978, doi:10.1175/2010JHM1206.1.

Tuttle, J. D., R. E. Carbone, and P. A. Arkin, 2008: Comparison of ground-based radar and geosynchronous satellite climatologies of warm-season precipitation over the United States. *J. Appl. Meteor.*, **47**, 3264–3270, doi:10.1175/2008JAMC2000.1.

Ushio, T., and Coauthors, 2009: A Kalman filter approach to the Global Satellite Mapping of Precipitation (GSMaP) from combined passive microwave and infrared radiometric data. *J. Meteor. Soc. Japan*, **87A**, 137–151, doi:10.2151/jmsj.87A.137.

Villarini, G., and W. F. Krajewski, 2007: Evaluation of the research version TRMM three-hourly 0.25° × 0.25° rainfall estimates over Oklahoma. *Geophys. Res. Lett.*, **34**, L05402, doi:10.1029/2006GL029147.

——, R. Goska, J. Smith, and G. Vecchi, 2014: North Atlantic tropical cyclones and U.S. flooding. *Bull. Amer. Meteor. Soc.*, **95**, 1381–1388, doi:10.1175/BAMS-D-13-00060.1.

Wu, H., R. F. Adler, Y. Hong, Y. Tian, and F. Policelli, 2012: Evaluation of global flood detection using satellite-based rainfall and a hydrologic model. *J. Hydrometeor.*, **13**, 1268–1284, doi:10.1175/JHM-D-11-087.1.

Xie, P., and A.-Y. Xiong, 2011: A conceptual model for constructing high-resolution gauge–satellite merged precipitation analyses. *J. Geophys. Res.*, **116**, D21106, doi:10.1029/2011JD016118.

——, A. Yatagai, M. Chen, T. Hayasaka, Y. Fukushima, C. Liu, and S. Yang, 2007: A gauge-based analysis of daily precipitation over East Asia. *J. Hydrometeor.*, **8**, 607–626, doi:10.1175/JHM583.1.

Yatagai, A., K. Kamiguchi, O. Arakawa, A. Hamada, N. Yasutomi, and A. Kitoh, 2012: APHRODITE: Constructing a long-term daily gridded precipitation dataset for Asia based on a dense network of rain gauges. *Bull. Amer. Meteor. Soc.*, **93**, 1401–1415, doi:10.1175/BAMS-D-11-00122.1.

Yong, B., L.-L. Ren, Y. Hong, J.-H. Wang, J. J. Gourley, S.-H. Jiang, X. Chen, and W. Wang, 2010: Hydrologic evaluation of multisatellite precipitation analysis standard precipitation products in basins beyond its inclined latitude band: A case study in Laohahe basin, China. *Water Resour. Res.*, **46**, W07542, doi:10.1029/2009WR008965.

——, and Coauthors, 2013: First evaluation of the climatological calibration algorithm in the real-time TMPA precipitation estimates over two basins at high and low latitudes. *Water Resour. Res.*, **49**, 2461–2472, doi:10.1002/wrcr.20246.

——, and Coauthors, 2014: Intercomparison of the version-6 and version-7 TMPA precipitation products over high and low latitudes basins with independent gauge networks: Is the newer version better in both real-time and post-real-time analysis for water resources and hydrologic extremes? *J. Hydrol.*, **508**, 77–87, doi:10.1016/j.jhydrol.2013.10.050.

——, D. Liu, J. J. Gourley, Y. Tian, G. J. Huffman, L.-L. Ren, and Y. Hong, 2015: Global view of real-time TRMM Multisatellite Precipitation Analysis: Implications for its successor global precipitation measurement mission. *Bull. Amer. Meteor. Soc.*, **96**, 283–296, doi:10.1175/BAMS-D-14-00017.1.

You, Y., and G. Liu, 2012: The relationship between surface rainrate and water paths and its implications to satellite rainrate retrieval. *J. Geophys. Res.*, **117**, D13207, doi:10.1029/2012JD017662.

——, N.-Y. Wang, and R. Ferraro, 2015: A prototype precipitation retrieval algorithm over land using passive microwave observations stratified by surface condition and precipitation vertical structure. *J. Geophys. Res. Atmos.*, **120**, 5295–5315, doi:10.1002/2014JD022534.

Yu, Z., H. Yu, P. Chen, C. Qian, and C. Yue, 2009: Verification of tropical cyclone-related satellite precipitation estimates in mainland China. *J. Appl. Meteor. Climatol.*, **48**, 2227–2241, doi:10.1175/2009JAMC2143.1.